


True Material Selection in a Liquid Phase Epitaxy System for Growth of High- T_c Superconducting Films

Yılmaz Şimşek^{1,2} 

¹Sabancı University Nanotechnology Research and Application Center, Istanbul, Türkiye, ysimsek@sabanciuniv.edu, ror.org/049asqa32

²Sabancı University, Faculty of Engineering and Natural Science, Istanbul, Türkiye, ror.org/049asqa32

ARTICLE INFO

ABSTRACT

Keywords:

High- T_c superconductors
Bi-2212 epitaxial films
Liquid phase epitaxy
Corrosion effects
Material inertness in KCl melt



Article History:

Received: 09.09.2025

Revised: 18.11.2025

Accepted: 03.12.2025

Online Available: 30.01.2025

The chemical stability of liquid-phase epitaxy (LPE) materials plays a decisive role in the quality of high-temperature $\text{Bi}_2\text{Sr}_2\text{Ca}_{n-1}\text{Cu}_n\text{O}_{2n+4+\delta}$ (BSCCO) superconducting films. In this study, the corrosion and dissolution behavior of two commonly used crucibles (made of Pt, and Pt-Rh alloy) and two substrates (MgO and NdGaO_3) in BSCCO/KCl solution were systematically investigated during the growth of $\text{Bi}_2\text{Sr}_2\text{CaCu}_2\text{O}_{8+\delta}$ (Bi-2212) films. Corrosion effects observed by optical and SEM imaging on the Pt–Rh crucible and NdGaO_3 substrate led to a detailed investigation of impurity incorporation into the films. The presence and origin of these impurities were identified by SEM-EDS, while their influence on the crystal structure and superconducting properties was evaluated using XRD and SQUID magnetometry, respectively. Imaging and elemental analysis show that films incorporating impurity atoms from the substrate exhibit degraded texture, correlated with the solubility of the surface material. This degradation is further accompanied by a marked suppression of superconductivity, arising from the combined effects of extrinsic impurities and the compromised microstructure. Overall, the findings underscore the critical importance of LPE material's inertness in controlling impurity incorporation and preserving both the textural integrity and superconducting behavior of LPE-grown Bi-2212 films. This work provides essential insights into impurity–flux interactions and highlights pathways to improve the reproducibility and quality of epitaxial Bi-2212 film growth.

1. Introduction

There are only three well-established superconducting phases within Bi-based cuprate family commonly represented by the general formula $\text{Bi}_2\text{Sr}_2\text{Ca}_{n-1}\text{Cu}_n\text{O}_{2n+4+\delta}$ (BSCCO). Here n (>1) denotes the number of Cu-O planes between the alternating Bi-O/Sr-O layers and δ indicates oxygen excess level associated with chemical doping state of the material. In a first sequential series of the n number, superconducting BSCCO phases and their superconducting transition temperatures (T_c) are listed as follows: $n = 1 \rightarrow \text{Bi}_2\text{Sr}_2\text{CuO}_{6+\delta}$ (Bi-2201) with $T_c \leq 20$ K; $n = 2 \rightarrow \text{Bi}_2\text{Sr}_2\text{CaCu}_2\text{O}_{8+\delta}$ (Bi-2212) with $T_c \leq 90$ K; $n = 3 \rightarrow \text{Bi}_2\text{Sr}_2\text{Ca}_2\text{Cu}_3\text{O}_{10+\delta}$ (Bi-2223) with $T_c \leq 110$ K [1, 2]. For $n = 4$, Bi-2234 shows also a

superconductivity below 104 K but it has not been studied well due to its complex phase control and marginal benefit compared to Bi-2223 [3].

Each of these phases exhibits a pseudo-tetragonal crystal structure ($a \approx b \neq c$) with in-plane lattice parameters (a and b) of approximately 5.4 Å. While the lattice dimensions along the a – b plane remain nearly constant, the c -axis lattice parameter increases with the number of Cu–O planes (i.e., the value of n), with typical values of approximately 24.5 Å, 30.7 Å, and 37.1 Å for Bi-2201, Bi-2212, and Bi-2223, respectively [4, 5]. For instance, the unit cell of Bi-2201 contains single superconducting Cu–O planes, while Bi-2223 consisting of three superconducting layers

separated by intervening Ca atomic planes thereby exhibits the largest lattice parameter along the c- axis.

Intrinsic Josephson junctions (IJJ) are remarkable characteristics of superconducting BSCCO materials exhibiting strong anisotropy and short coherence lengths [6]. These materials naturally consist of alternating stacks of superconducting Cu-O/Ca and insulating Bi-O/Sr-O layers, well aligned along the c-axis. These superconductor–insulator–superconductor multilayers are called intrinsic Josephson junctions (IJJs) providing a versatile platform for developing various superconducting devices based on Josephson effects [7, 8]. Among these superconducting BSCCO materials, Bi-2212 crystals are mostly preferred to study IJJ effects due its pure crystalline growth feasibility, high temperature transition (T_c), and more familiar properties. Usually Bi-2212 crystals are utilized to realize THz components such as THz radiation source, detectors, waveguides and high-band width receivers and to promote novel approaches through high- T_c quantum circuits such as superconducting quantum interference devices and qubits, and logics. To advance a wide-range of applications of IJJs, impurity-free, high crystalline quality and large-scale growth of Bi-2212 platforms are highly required. Due to growth limits in size of bulk crystals and the necessity of good thermal link with the cryogenic system, large scale production of high-quality Bi-2212 films is of great importance in the development of superconducting platforms for advance electronic applications.

Liquid phase epitaxy (LPE) is a highly effective technique for the epitaxial growth of both thin and thick films across a broad range of material classes, including oxides, magnetic, and optical materials [9-11]. It has also been employed for successfully growing high-quality, thick and crystalline high- T_c superconducting films like $\text{Bi}_2\text{Sr}_2\text{CaCu}_2\text{O}_{8+\delta}$ (Bi-2212) [9, 12-14]. A key advantage of LPE lies in its simplicity, scalability, and ability to produce high-quality Bi-2212 films with high growth rates without the need for costly or complex equipment [9-11]. The basic setup required for LPE consists of a crucible, a vertical furnace, a substrate holder, motion stages, and components, sufficient to

support epitaxial film growth [13-16]. At elevated temperatures, but still below the melting point of the precursor material, the high mobility of dissolved components in the liquid medium promotes self-nucleation and epitaxial crystallization on a compatible substrate. Successful LPE growth relies on optimizing several critical parameters, including the growth temperature, supersaturation conditions of the LPE solution, and temperature gradient that facilitates the upward transport of solute toward the substrate. However, material section is just as important as systematic system optimization.

The KCl flux with BSCCO components forms an aggressive solution which leads to corrosion damages on the surface of many materials at high temperatures. This high-temperature corrosion occurs when surface elements of the LPE tools chemically react with components of the KCl/BSCCO molten solution to form new compounds with melting points below the ambient temperature. These newly formed compounds, along with material from the setup itself, may then dissolve into the LPE solution, leading to contamination. Therefore, the careful selection of materials used in the construction of the LPE apparatus is crucial to eliminate corrosion and ensure the sustainable LPE growth. Besides the chemical stability, it is also important for high-quality impurity-free Bi-2212 films. For instance, impurities originating from LPE apparatus components and dissolving into the BSCCO melt can significantly influence nucleation, disrupt the epitaxial crystalline growth, or become incorporated into the film lattice, ultimately suppressing the superconducting performance of Bi-2212 films.

This work systematically evaluates the chemical stability of LPE components such as substrates, crucibles, sample holders, and thermocouples which are exposed to the aggressive Bi-2212/KCl solution under standard high- T_c film growth conditions. Here we focus on the durability of MgO (100) and NdGaO_3 (001) substrates, selected for their favorable lattice match. Additionally, an LPE growth experiment was performed on a Si substrate to demonstrate severe corrosion at high temperature. The stability of Pt–Rh (10%) alloy crucibles, widely

used due to its high melting point (~ 1800 °C), is also compared besides that of pure Pt.

Chemical stability of all these materials was examined through surface morphology of the LPE accessories and crystal structure and stoichiometry of the as-grown films as well as their superconducting transition temperature and film stoichiometry using optical microscopy, scanning electron microscopy (SEM), X-ray diffraction (XRD), energy-dispersive X-ray spectroscopy (EDS), and magnetization measurements. This study provides a direct framework for selecting chemically inert, lattice-compatible materials to enable reproducible, high-quality Bi-2212 film growth.

2. Experimental

To grow Bi-2212 films using LPE, the well-established protocol is followed as described in [13-16]. Figure 1 presents images of the prepared precursor materials and molten KCl flux, as well as a schematic illustration of the LPE growth mechanism. As a first step, the precursor mixture is prepared using Bi_2O_3 , SrCO_3 , CaCO_3 , and CuO powders in specific molar ratios. In this study, both Bi-2212 and Bi-2223 stoichiometries were employed. Approximately 20 g of this powder mixture is thoroughly ground in an agate mortar to ensure homogeneity and fine particle size, which is crucial for uniform melting and consistent chemical reactivity in subsequent steps.

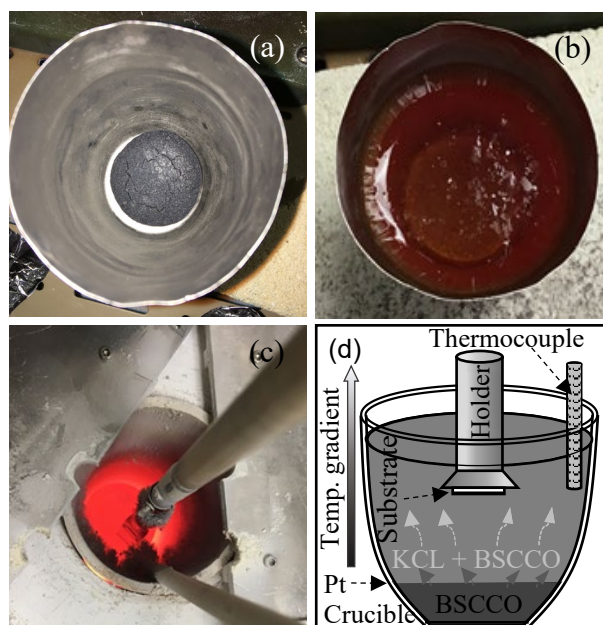


Figure 1. Process images from the LPE growth of Bi-2212 superconducting films: (a) BSCCO precursor at the crucible bottom after air quenching, (b) pre-melted KCl flux covering the precursor during air quenching, (c) view of the LPE furnace during Bi-2212 film growth, and (d) schematic illustration of the liquid phase epitaxy technique

The ground powder is then placed in a platinum crucible and calcined at 850 °C for 1 hour to decompose residual carbonates. Immediately after calcination (see Figure 1(a)), the material is rapidly quenched to room temperature to obtain an amorphous BSCCO form at the bottom of the crucible. Next, 100 g of high-purity KCl is added onto the quenched precursor and, the KCl/BSCCO mixture is reheated to 800 °C for 1 hour, and then rapidly cooled down. Figure 1(b) shows the appearance of the pre-melted KCl flux with the BSCCO precursor during the cooling process. In the LPE process, KCl acts as a low-viscosity flux, providing dissolution of BSCCO components below the melting point, enhancing solute mobility and thereby supporting the growth of high-quality epitaxial films [13, 17].

The crucible containing the KCl/Bi-2223 pre-molten material is closed with a lid and placed at the position of the hot zone of the vertical furnace where an ideal temperature gradient had been optimized. The system was held at 870 °C for at least 10 hours to produce a supersaturated solution capable of depositing epitaxial films. Once the desired LPE growth conditions are established, a substrate attached to a platinum holder was slowly lowered from the top of the

furnace into the molten solution. The substrate was positioned 5–10 mm below the liquid surface and maintained there during the growth period. Figure 1(c) shows a top view of the setup when the holder was in the LPE growth position. Due to the vertical temperature gradient, solute transport occurs from the bottom of the crucible upward, allowing BSCCO components to crystallize on the relatively cooler surface of the substrate. The schematic illustration in Figure 1(d) shows this LPE growth mechanism, where dissolved BSCCO components are driven by upward gradient to the top surface of the flux.

In this study, a series of LPE growth experiments were carried out in the same KCl/BSCCO solution with a 5:1 weight ratio at 870°C on MgO (100), NdGaO₃ (001), and Si (100) substrates within two different crucible made of Pt-Rh(10%) alloy and pure Pt. Chemical stability and/or corrosion behavior of LPE materials including substrates and crucibles have been investigated through their surface morphologies and textures of as-grown films in the first experimental series using SEM and optical microscope. The second part of LPE experiments focusing on impurity incorporation into the films and its impact on superconducting properties, analyzed using XRD, EDS, and SQUID magnetometry. For this purpose, systematic LPE growth experiments were conducted using Pt–Rh alloy and pure Pt crucibles with both MgO and NdGaO₃ substrates. All films were prepared during the first or second growth run from each melt to minimize precursor aging effects. Key growth parameters, along with the substrate and crucible materials used in these experiments (films B-29, B-21, B-22, and B-23), are summarized in Table 1. In the first two series carried out with Pt–Rh crucibles, the first films grown on NdGaO₃ substrates are labeled B-29 and B-21, respectively. In the subsequent run of the second series, film B-22 was grown on an MgO substrate. Finally, film B-23 an impurity-free growth was achieved in the third series using a pure Pt crucible and an MgO substrate.

Table 1. Key growth parameters and substrate/crucible materials for films obtained in different LPE growth sets

Film/ Run#	Precursor comp.	Growth temp. (°C)	Material	
			Subst.	Crucible
Bi-29 1 st	Bi-2212	873	NdGaO ₃	Pt- 10%Rh
Bi-21 1 st	Bi-2212	872	NdGaO ₃	Pt- 10%Rh
Bi-22 2 nd	Bi-2212	886	MgO	Pt- 10%Rh
Bi-23 1 st	Bi-2223	872	MgO	Pure Pt

Growth conditions for all films were kept nearly identical, aside from intentional variations in specific parameters. For instance, films B-29, B-21, and B-22 were grown from a Bi-2212 precursor composition; however, the growth temperature was raised for film B-22 in order to evaluate the chemical stability of the MgO substrate above 870 °C, which was previously established as optimal for obtaining high-quality epitaxial Bi-2212 films. In contrast, film B-23 was grown under well-established LPE conditions with a Bi-2223 precursor and a growth temperature, serving as a high-quality reference film for comparison with the others.

3. Results and Discussion

The results obtained from two different experimental series are presented under four subheadings. The first part addresses the durability of the materials used in LPE growth and the texture of the films in relation to corrosion effects. The compositional and structural characteristics of the resulting films are presented together in the second part, followed by a separate section describing their superconducting properties. Finally, the last section integrates and discusses all findings in a comprehensive manner.

3.1. Corrosive effects of the KCl/BSCCO solution on LPE tools and film morphology

The chemical inertness (i.e., corrosion rate) of LPE materials strongly depends on the synthesis temperature, the solute concentration, and the

nature of dissolved components and flux elements present in the molten solution. Therefore, the chemical durability of LPE tools must be evaluated under the standard conditions required for the epitaxial growth of high-quality Bi-2212 films. Figure 2 presents surface images of substrates, crucibles, and the substrate holder. To intentionally demonstrate the corrosive effect of the KCl/BSCCO solution, a single LPE growth experiment was performed on a Si substrate, in spite of its chemical instability in molten flux [18].

As shown in Figure 2(a), the Si substrate was severely corroded in the melt. In this study, the chemical resistance of MgO and NdGaO₃ (NGO), which are the two most commonly used substrates in LPE growths of Bi-2212 films, was tested. Among them, [001]-oriented NGO is generally preferred due to its closer lattice match with Bi-2212 crystals. However, pit-like structures were observed on the NGO surface as a result of erosion in the LPE medium. Figure 2(b) illustrates partial surface damage on the NGO substrate. Despite this, regions of the NGO surface initially protected by film coating still enabled the formation of continuous epitaxial layers.

To highlight the corrosion effect, the as-grown film was removed by rinsing in HCl/H₂O (10:1), exposing the underlying erosion. In contrast, although the lattice compatibility of MgO with Bi-2212 is not as favorable as that of NGO, MgO demonstrated excellent chemical stability in a series of LPE experiments. Figure 2(c) shows the undamaged surface of a (100)-oriented MgO substrate after 10 hours in the molten solution.

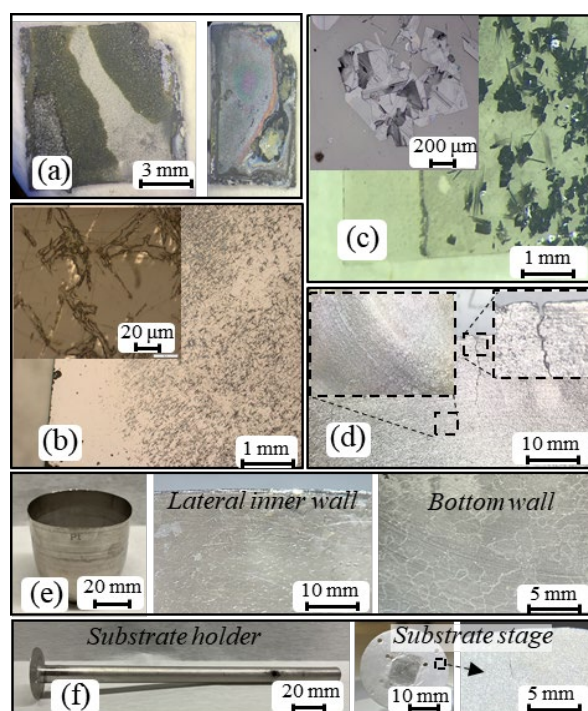


Figure 2. Surface morphologies of substrates, Si (a), NdGaO₃ (b), and MgO (c), after ~10 h of LPE growth at 870–880 °C. In some cases, the Bi-2212 film was removed using an HCl/H₂O solution to reveal the substrate surface. (d) Surface images of Pt–Rh (10%) crucibles after repeated use in a series of growth experiments. Views of pure platinum crucibles (e) and the platinum substrate holder (f) following multiple liquid phase epitaxy growth experiments

Beyond substrates, the chemical durability of other components such as the substrate holder, clips, and thermocouple, periodically kept in the molten solution, is also crucial for sustainable LPE film growths. For example, the crucible material, in particular, must reliably contain the KCl/BSCCO melt throughout the growth series. In an initial series of the growth experiments, a crucible made of Pt–Rh (10%) alloy was employed due to its higher melting point compared to that of pure platinum. However, it has been observed that while the inner wall of the crucible corroded overtime, other tools out of pure platinum, including the substrate holder, clips, and thermocouple cover, remained chemically stable. Figure 2(d) reveals a surface corrosion and additionally a partial crack on the surface of the Pt–Rh crucible. As demonstrated, surface corrosion significantly compromises the durability of experimental equipment, but also releases impurities into the melt which may subsequently be incorporated into the film composition. The Pt–Rh alloy

crucible showed corrosion and cracks, whereas the pure platinum crucible was chemically inert inside the BSCCO/KCl melt. Figure 2(e) and (f) display the uncorroded surfaces of a crucible and holder, both made of pure platinum.

Notably, polygonal grain-like patterns were observed on the Pt crucible surface as seen in Figure 2(e). These patterns, particularly distinct at the crucible bottom, exhibit surface faceting and grain-boundary relief. According to the literature [19], such features arise from recrystallization and grain growth of platinum induced by heat treatment at 0.3–0.5 times its melting point. On the sample holder, however, these granular patterns appeared smaller and less pronounced, as it was not subjected to prolonged heat treatment in the presence of BSCCO components.

In addition to crystal compatibility, the chemical inertness of the substrate plays a critical role in epitaxial film growth. For instance, epitaxial film formation either may be completely disabled in the presence of severe corrosion, or may result in more mosaic complex texture depending on the solubility degree of the substrate material. Figure 3 exhibits epitaxial textures of Bi-2212 films grown on NdGaO_3 (001) and MgO (100) substrates in the alloyed and pure Pt crucibles which are representing contaminated and impurity-free LPE growths respectively.

As can be seen in Figure 3(a), despite a partial corrosion on the NdGaO_3 substrate, an epitaxial film still develops across its entire surface. Similarly, a continuous Bi-2212 film uniformly covers the surface of MgO substrate (see Figure 3(b)). However, the film on NdGaO_3 , reveals a mosaic-textured morphology with randomly oriented small grains due to surface corrosion, whereas the chemically inert MgO supports a more uniform and large-grain texture. This is related to the surface durability supporting continuous and uniform film formation. More clearly, the initially formed Bi-2212 islands shield the underlying surface areas from the damaging, while uncoated regions are gradually deteriorated under the corrosion effect of BSCCO/KCl melt that results in corrosion pits on the substrate as shown in Figure 2(b). Owing to the persistent LPE growth mechanism, the

advancing film not only continues across the substrate but also overgrows corrosion pits, where the gaps are bridged by irregular, mosaic-like crystalline domains. Thus, film texture becomes more mosaic with randomly oriented smaller grains depending on the surface damaging. It is so pronounced that the longer the exposure time in the aggressive solution, the more damage will occur to the substrate surface.

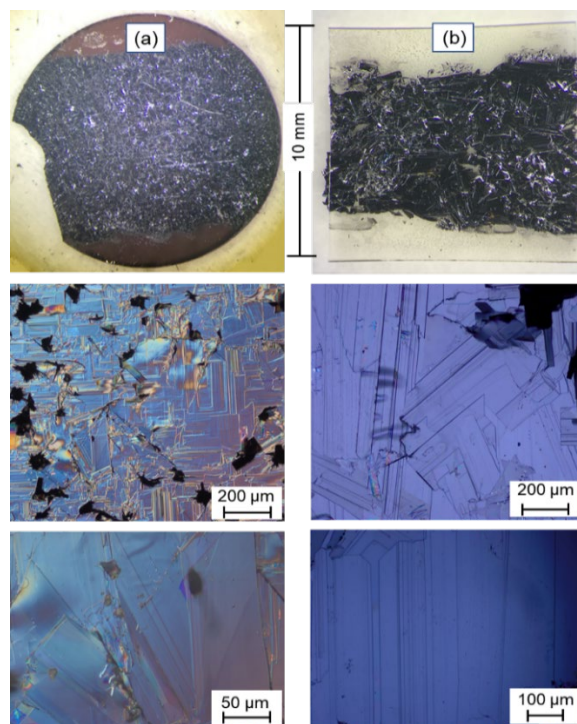


Figure 3. Optical images of Bi-2212 epitaxial films grown on NdGaO_3 (a) and MgO (b) substrates under the standard LPE conditions

In addition, continuous epitaxial formation with large-grain texture can be favored by high growth rate depending on the supersaturation of LPE solution, upward transportation of solutes, and the cooling rate of the substrate on the long holder. Usually the first sets of LPE experiments provide high growth rate conditions for complete coverage of the epitaxial film texture across the entire degraded substrate (see Figure 3(a)). Under degraded conditions following sequential LPE growth runs, the substrate surface exhibits severe degradation as a result of extended exposure to the aggressive solution as seen in Figure 2(b).

3.2. Compositional and structural analyses of LPE films

In the next step, the crystal structures, elemental compositions, and superconducting properties of the films grown in three different LPE experimental series, where impurity contamination was progressively reduced, were systematically characterized using XRD, EDS, and SQUID magnetometry. To minimize precursor aging effects, all films were prepared during the first or second growth run from each melt.

EDS spectra of the films and the corresponding atomic percentages of the major elements are presented in Figure 4. In addition to the expected Bi, Sr, Ca, Cu, and O signals, Ga and Rh impurities were detected in films B-29 and B-21, originating from dissolution of the NdGaO₃ substrate and the Pt–Rh crucible, respectively (see Figure 4(a) and (b)). Rh impurities were detected only in trace amounts within the films. Indeed, it could not be found in sample B-22. In contrast, Ga originating from the substrate was incorporated into the films at significantly higher levels which were approximately 2.5% and 11% for films B-29 and B-21 respectively. This clearly indicates that Ga dissolves into the melt much more readily than Rh. The MgO-based film B-22 exhibited only Rh contamination from the crucible wall, while the substrate surface remained chemically stable in the LPE medium (second spectrum from the top). In contrast, the spectrum of film B-23, grown on an MgO substrate within a pure Pt crucible, shows no peaks attributed to extrinsic impurities (bottom spectrum in Figure 4(a)). In addition to the corrosion-related impurities, a relatively high level of carbon contamination was also observed in films B-29, B-21, and B-22. Such carbon contamination is typically detected in EDS analyses of LPE-grown films, although it was not evident in the EDS data of sample B-23. This contamination is likely caused by electron-beam interactions with residual carbon either adsorbed on the film surface or present in the SEM chamber [20], and/or by incorporation of carbon residues from the precursor into the film during upward transport of BSCCO components.

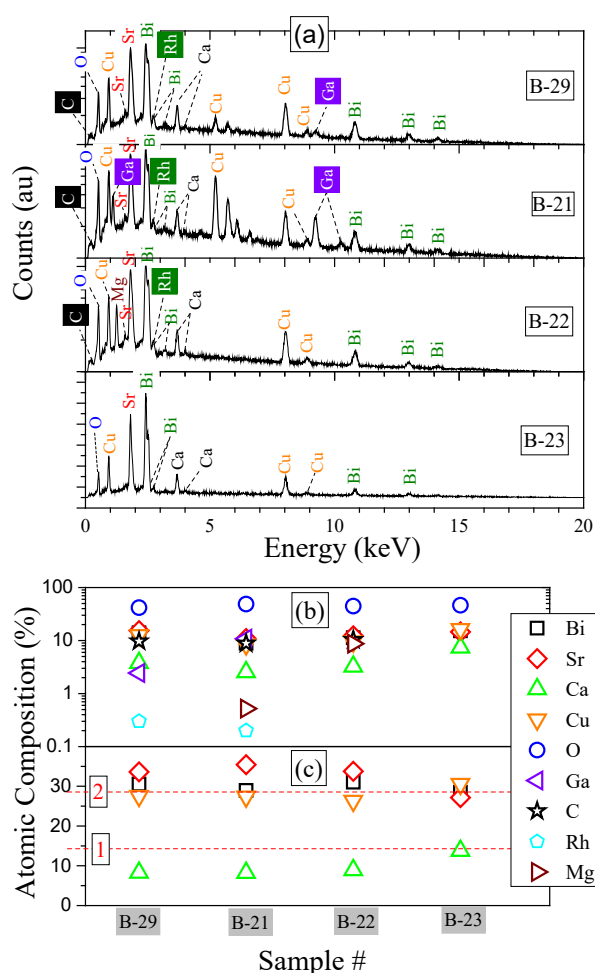


Figure 4. EDS patterns of LPE films grown under approximately the same LPE conditions on NdGaO₃ (B-29, and B-21)) and MgO (B-22, and B-23) substrates (a). Film B-23 was only grown using pure platinum crucible, while the other films (B-22, B-21 and B-29) were obtained in separate LPE experiments performed in Pt-Rh crucible. Atomic percentages of all detected elements (b) and the major constituent elements of Bi-2212 (Bi, Sr, Ca, Cu) (c) in the films. Dashed lines represent the stoichiometry of Bi-2212 single phase

Figure 4(c) summarizes the atomic percentages of Bi, Sr, Ca, and Cu for each film, together with dashed lines representing the nominal elemental ratios of Bi-2212 single crystals. The EDS data for films B-29, B-21, and B-22, all grown from a Bi-2212 precursor, show notable deviations from the nominal Bi-2212 stoichiometry, particularly reduced Ca and Cu contents, which can be attributed to their limited solubility in the molten KCl flux [14, 16]. In contrast, film B-23, prepared using a Bi-2223 stoichiometric precursor enriched in Ca and Cu, exhibits an elemental distribution much closer to the ideal Bi-2212 composition.

XRD patterns of the films are displayed in Figure 5. With the exception of film B-22, the diffraction peaks are predominantly consistent with the Bi-2212 phase, accompanied by minor reflections from the Bi-2201 phase (magnified using logarithmic scaling). Notably, in the B-22 film, the Bi-2201 secondary phase constitutes nearly 93.5% of the volume fraction. This is attributed to the elevated growth temperature for testing MgO chemical stability.

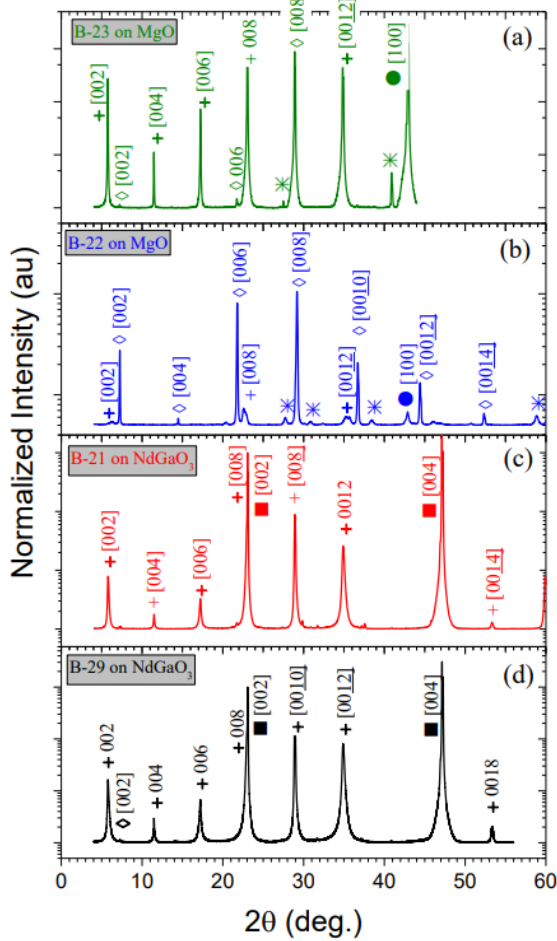


Figure 5. X-ray 2θ scans of epitaxial films (B-23, B-22, B-21, and B-29) grown on MgO substrates (a, b) and NdGaO₃ substrates (c, d). The diffraction patterns exhibit sharp reflections corresponding to the Bi-2212 (+) and Bi-2201 (◇) phases. Peaks originating from the MgO and NdGaO₃ substrates are marked with ● and ■, respectively. The symbol * denotes surface-related contaminations on the substrates

The c-axis lattice parameters of the films were precisely determined using the Nelson–Riley method, which is widely employed to minimize systematic errors in XRD measurements such as specimen displacement, transparency effects, and instrumental aberrations. This approach

relies on extrapolating the lattice parameters obtained from individual reflections as a function of the Nelson–Riley function [21], defined as:

$$F(\theta) = \frac{1}{2} \left[\frac{\cos^2 \theta}{\sin \theta} + \frac{\cos^2 \theta}{\theta} \right] \quad (1)$$

The lattice parameters were calculated from the general orthorhombic relation:

$$\frac{1}{d_{hkl}^2} = \frac{h^2}{a^2} + \frac{k^2}{b^2} + \frac{l^2}{c^2} \quad (2)$$

where, d_{hkl} is the interplanar spacing obtained from each reflection with Miller index (h , k , and l) using Bragg's law:

$$n\lambda = 2d_{hkl} \sin \theta \quad (3)$$

Here, λ is the x-ray wavelength, and n is the diffraction order in Eq. (3).

Figure 6 shows the variation of the c-axis lattice constants versus the Nelson-Riley function (Eq. (1)) for Bi-2212 and Bi-2201 phases which were calculated from the XRD result of each film. They reveal near-linear dependences demonstrating the consistent correction of the systematic errors across all reflections. The true c-axis lattice parameters of Bi-2212 in the film structures were determined from the extrapolated intercept of Nelson-Riley plots at $F(\theta) = 0$ (see Figure 6(a)). Thus, the c-axis values for films B-29, B-21, B-22, and B-23 were found to be 30.92 Å, 30.94 Å, 31.12 Å, and 30.93 Å, respectively, which are consistent with literature values [5]. Typically, slight variations in Bi-2212 stoichiometry, as well as in its oxygen content, lead to small deviations in the lattice parameter along the c-axis [22, 23]. However, the unusually large extension of the c-axis parameter observed here may result from non-uniform intergrowth of the minor Bi-2212 phase within the crystalline layers of the dominant Bi-2201 phase [24].

In Figure 6(b) the lattice constant of the major Bi-2201 phase in film B-22 was found to be 24.49 Å, in good agreement with literature values [1].

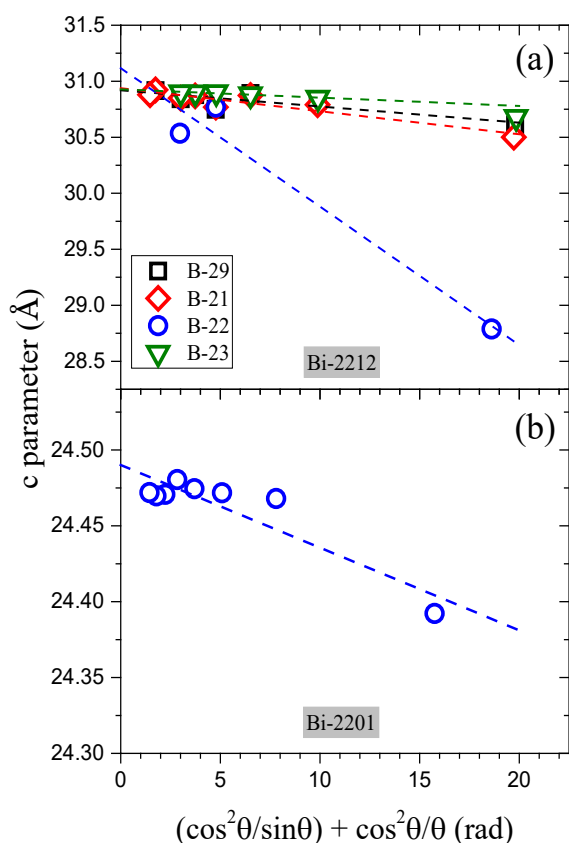


Figure 6. The c-axis parameter analysis in XRD patterns of the films corresponding to Bi-2212 (a) and Bi-2201 (b) phases using Nelson-Riley extrapolation method

3.3. Magnetic characterization of LPE superconducting films by SQUID

Superconducting properties of the films were evaluated using magnetization measurements in a SQUID magnetometer under an applied field of 1 G during warming up, after zero-field cooling. Figure 7 depicts their normalized magnetic moment versus temperature (M-T) curves evaluated from their raw M-T data plotted in the inset. The B-23 film, prepared under the optimum LPE conditions with chemically stable materials, exhibit a M-T change with a sharp superconducting transition at ~ 80 K, with uniform and stable magnetization below T_c . By contrast, M-T curves of films B-29, B-21, and B-22 display broader transitions starting near 70 K, with non-saturating magnetization curves, indicating structural inhomogeneities and impurity effects.

3.4. Impurity sources and their effects on the superconducting properties of LPE films

The presence of Ga and Rh impurities in the films is attributed to their partial dissolution from the NdGaO_3 substrate and the Pt-Rh crucible, respectively, through low-temperature chemical interactions at the solid-flux interface. In molten solutions, such dissolution corrosion can occur either via metallurgical alloying or via chemical reaction, depending on the local environment. The Rh loss at the crucible surface specifically indicates an alloying-driven interaction. Among the binary combinations of Rh with elements present in the BSCCO/KCl system, the Rh-Bi phase diagram shows a low eutectic temperature (~ 260 °C) [25], far below the typical growth temperature of ~ 870 °C. Since metallic Bi may be present in the KCl melt in various solute forms, Rh can be incorporated into the flux via the low-melting Rh-Bi eutectic pathway. This alloying effect is therefore considered the most credible mechanism for crucible corrosion under our conditions. In fact, ensuring the proper use of Pt and Pt-alloy crucibles remains a major challenge in industrial applications [26].

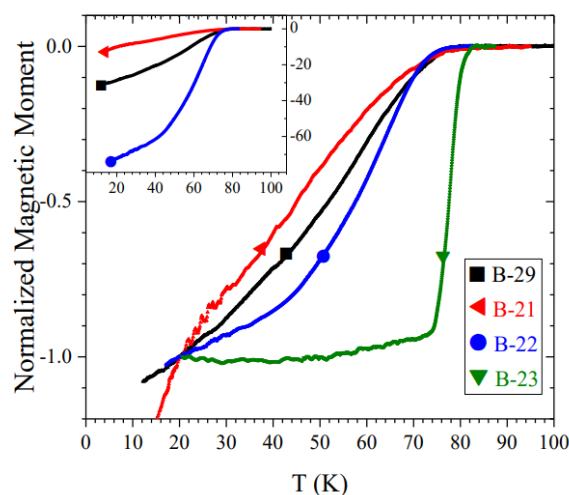


Figure 7. Normalized magnetic moment (M-T) of the LPE films measured during warming up in the SQUID magnetometer. The inset displays the corresponding raw M-T curves

In contrast, Ga contamination originates primarily from chemically reactive dissolution, whereby surface Ga^{3+} is extracted from NdGaO_3 and stabilized in the flux as volatile or soluble Ga-chloride complexes. Despite ineffective chlorination of Rh or Rh-O compound by KCl [27], Ga readily forms solvated species such as

GaCl₃ in molten chloride media [28]. This flux-mediated leaching mechanism provides a favorable pathway for Ga transport into the solution and ultimately into the growing BSCCO films, illustrating the aggressive chemical environment imposed by the BSCCO/KCl system.

Impurities released from the corrosion of materials in the aggressive KCl melt are transported by the upward temperature gradient and incorporated into the growing films during nucleation on the cooler substrate surface. Such incorporated impurities can significantly suppress the superconducting properties of Bi-2212 films [29]. For example, although films grown on NdGaO₃ (B-29 and B-21) exhibit similarly high fractions of the Bi-2212 phase, the magnetization of film B-21 is noticeably lower due to its substantially higher Ga impurity content (see Figure 7). This indicates that the corroded substrate surface serves as a proximal source for impurity incorporation into the films.

In addition, as the surface morphology of the substrate deteriorates in the aggressive molten environment, the epitaxial film tends to form more complex textures consisting of overlapping smaller grains. The grain size in the films grown on NdGaO₃ is not small enough to strongly suppress superconductivity. However, the smaller the grain size, the greater the number of grain boundaries, making the quality of intergrain coupling critical for establishing robust bulk superconductivity. It is well known that poor grain connectivity can significantly suppress superconductivity [30]. Consequently, the broadened and weakened superconducting transition observed in the magnetization curves of films B-29 and B-21 can be attributed to both Ga impurity incorporation and poor intergrain coupling within their small-size grain textures.

The magnetization of these films is even lower than that of the two-phase film (B-22) grown on MgO. Although B-22 predominantly consists of Bi-2201 phase according to XRD, it exhibits a broad superconducting transition starting near 70 K, indicative of a dominant Bi-2212-like behavior. As is well known, the Bi-2201, Bi-2212, and Bi-2223 phases, distinguished by their distinct numbers of CuO₂ layers ($n = 1, 2,$ and 3

respectively), may readily coexist as a multiphase mixture in BSCCO films, and each has its own impact on the resulting superconducting properties. Occasionally, additional CuO₂ layers intergrow within the matrix. These intergrowths form locally segregated regions whose superconducting behavior corresponds to that of a BSCCO phase with the same effective number of CuO₂ layers [13, 14]. For film B-22, the presence of extra CuO₂ layers intergrown within the Bi-2201 matrix likely enhances the magnetization signal by inducing a Bi-2212-like superconducting response. Because these additional CuO₂ layers do not accumulate in a fully ordered sequence, they may not be clearly visible in the XRD patterns. However, the EDS result of B-22 shows nearly the same elemental stoichiometry as films B-29 and B-21. This suggests that numerous intergrown extra CuO₂ layers in addition to trace amounts of Bi-2212 are present within the film. This can account for the strong Bi-2212-like signal observed in the magnetization measurements.

In contrast, film B-23 exhibits a sharp superconducting transition at 75–80 K because it contains no measurable impurity atoms and possesses a high-quality Bi-2212 texture with large-size grains. Only the film shows a T_c significantly lower than the optimal value of ~90 K due to its reduced oxygen content. Altogether, these observations highlight the critical importance of the chemical stability of the materials, particularly the substrates, used in the LPE system.

4. Conclusion

In this study, corrosion effects of LPE materials were systematically investigated under well-established conditions for the growth of high-quality Bi-2212 films. It was found that the Pt–Rh crucible and the NdGaO₃ substrate underwent noticeable corrosion in the BSCCO/KCl melt, while the pure Pt crucible and the inert MgO substrate remained stable throughout the growth process. Trace impurities were detected in the films as a consequence of dissolution processes at the crucible and substrate interfaces. Specifically, Ga from NdGaO₃ and Rh from Pt–Rh crucibles were incorporated into the BSCCO

lattice, either through substitution at cation sites or by segregation at grain boundaries. Their presence was correlated with a significant suppression of the superconducting properties. Beyond impurity incorporation, substrate dissolution was found to alter the film microstructure, leading to more mosaic textures with overlapping smaller grains. This degradation in crystalline quality, combined with impurity effects, accounts for the observed reduction in superconducting performance. These results highlight the critical importance of chemical inertness in crucibles, substrates, and other LPE materials for controlling impurity incorporation and preserving the structural and functional quality of LPE-grown cuprate films.

Article Information Form

Funding

This work was partially supported by the Scientific and Technological Research Council of Türkiye (TÜBİTAK), with the project no: 219M454

The Declaration of Conflict of Interest/ Common Interest

No conflict of interest or common interest has been declared by the author.

Artificial Intelligence Statement

No artificial intelligence tools were used while writing this article.

Copyright Statement

The author owns the copyright of their work published in the journal and their work is published under the CC BY-NC 4.0 license.

References

- [1] J. Akimitsu, A. Yamazaki, H. Sawa, and H. Fujiki, "Superconductivity in the Bi-Sr-Cu-O system," *Jpn. J. Appl. Phys.*, vol. 26, no. 12A, pp. L2080-L2081, Dec 1987. doi: 10.1143/JJAP.26.L2080. [Online]. Available: <https://iopscience.iop.org/article/10.1143/JJAP.26.L2080>
- [2] H. Maeda, Y. Tanaka, M. Fukutomi, and T. Asano, "A new high-*t_c* oxide superconductor without a rare-earth element," *Jpn. J. Appl. Phys. Part 2-Lett.*, vol. 27, no. 2, pp. L209-L210, Feb 1988. doi: 10.1143/Jjap.27.L209. [Online]. Available: <https://iopscience.iop.org/article/10.1143/JJAP.27.L209>
- [3] T. Hatano, K. Kadowaki, and K. Nakamura, "Bi-2223 Bi-2234 superlattice - Its structural-analysis and superconducting transition-temperature," *Supercond. Superlattices Multilayers*, vol. 2157, pp. 207-210, 1994. doi: 10.1117/12.179173. [Online]. Available: <https://www.spiedigitallibrary.org/conference-proceedings-of-spie/2157/1/Bi-2223-Bi-2234-superlattice--its-structural-analysis-and/10.1117/12.179173.short>
- [4] Y. Matsui, H. Maeda, Y. Tanaka, and S. Horiuchi, "High-resolution electron-microscopy of modulated structure in the new high-*T_c* superconductors of the Bi-Sr-Ca-Cu-O system," *Jpn. J. Appl. Phys. Part 2-Lett.*, vol. 27, no. 3, pp. L361-L364, Mar 1988. doi: 10.1143/Jjap.27.L361. [Online]. Available: <https://iopscience.iop.org/article/10.1143/JJAP.27.L361>
- [5] S. A. Sunshine, et al., "Structure and physical properties of single crystals of the 84K superconductor $\text{Bi}_{2.2}\text{Sr}_2\text{Ca}_{0.8}\text{Cu}_2\text{O}_{8+\delta}$," *Phys. Rev. B*, vol. 38, no. 1, pp. 893-896, July 1988. doi: 10.1103/PhysRevB.38.893. [Online]. Available: <https://journals.aps.org/prb/abstract/10.1103/PhysRevB.38.893>
- [6] R. Kleiner, F. Steinmeyer, G. Kunkel, and P. Müller, "Intrinsic josephson effects in $\text{Bi}_2\text{Sr}_2\text{CaCu}_2\text{O}_8$ single crystals," *Phys. Rev. Lett.*, vol. 68, no. 15, pp. 2394-2397, Apr 1992. doi: 10.1103/PhysRevLett.68.2394. [Online]. Available: <https://journals.aps.org/prl/abstract/10.1103/PhysRevLett.68.2394>

- [7] I. Kakeya and H. B. Wang, "Terahertz-wave emission from Bi2212 intrinsic Josephson junctions: A review on recent progress," *Supercond. Sci. Technol.*, vol. 29, no. 7, p. 073001, July 2016. doi: 10.1088/0953-2048/29/7/073001. [Online]. Available: <https://iopscience.iop.org/article/10.1088/0953-2048/29/7/073001>
- [8] A. A. Yurgens, "Intrinsic Josephson junctions: recent developments," *Supercond. Sci. Technol.*, vol. 13, no. 8, pp. R85-R100, Aug 2000. doi: 10.1088/0953-2048/13/8/201. [Online]. Available: <https://iopscience.iop.org/article/10.1088/0953-2048/13/8/201>
- [9] C. Klemenz and H. J. Scheel, "Liquid-phase epitaxy of high-Tc superconductors," *J. Cryst. Growth*, vol. 129, no. 3-4, pp. 421-428, May 1993. doi: 10.1016/0022-0248(93)90476-D. [Online]. Available: <https://www.sciencedirect.com/science/article/abs/pii/002202489390476D?via%3Dihub>
- [10] H. J. Scheel, "Introduction to liquid phase epitaxy," in *Liquid Phase Epitaxy of Electronic, Optical and Optoelectronic Materials*, 2nd ed., P. Capper and M. Mauk, Eds. Hoboken, NJ, USA: John Wiley & Sons, 2007, pp. 1-19. doi: 10.1002/9780470319505.ch1. [Online]. Available: <https://onlinelibrary.wiley.com/doi/10.1002/9780470319505.ch1>
- [11] M. G. Mauk, "6 - Liquid-Phase Epitaxy," in *Handbook of Crystal Growth*, 2nd ed., T. F. Kuech, Ed. Boston, MA, USA: North-Holland, 2015, pp. 225-316. doi: 10.1016/B978-0-444-63304-0.00006-8. [Online]. Available: <https://www.sciencedirect.com/science/chapter/edited-volume/abs/pii/B9780444633040000068?via%3Dihub>
- [12] G. Balestrino, V. Foglietti, M. Marinelli, E. Milani, A. Paoletti, and P. Paroli, "Transport properties of epitaxial BSCCO films grown on untwinned NdGaO₃ substrates," *Solid State Commun.*, vol. 79, no. 10, pp. 839-841, Sept 1991. doi: [https://doi.org/10.1016/0038-1098\(91\)90316-N](https://doi.org/10.1016/0038-1098(91)90316-N). [Online]. Available: <https://www.sciencedirect.com/science/article/abs/pii/003810989190316N?via%3Dihub>
- [13] G. Balestrino, M. Marinelli, E. Milani, A. Paoletti, and P. Paroli, "Compositional dependence of properties of Bi_{2-y}Pb_ySr_{3-x}Ca_xCu₂O_{8+z} films grown by liquid phase epitaxy," *J. Appl. Phys.*, vol. 70, no. 11, pp. 6939-6944, Dec 1991. doi: 10.1063/1.349820. [Online]. Available: <https://pubs.aip.org/aip/jap/article-abstract/70/11/6939/390971/Compositional-dependence-of-properties-of-Bi2?redirectedFrom=fulltext>
- [14] Y. Simsek, et al., "Thick Bi₂Sr₂CaCu₂O_{8+δ} films grown by liquid-phase epitaxy for Josephson THz applications," *Supercond. Sci. Technol.*, vol. 31, no. 1, p. 015009, Jan 2017. doi: 10.1088/1361-6668/aa987e. [Online]. Available: <https://iopscience.iop.org/article/10.1088/1361-6668/aa987e>
- [15] G. Balestrino, V. Foglietti, M. Marinelli, E. Milani, A. Paoletti, and P. Paroli, "Epitaxial films of BSCCO grown from liquid KCl solutions onto several substrates," *IEEE Trans. Magn.*, vol. 27, no. 2, pp. 1589-1591, Mar 1991. doi: 10.1109/20.133488. [Online]. Available: <https://ieeexplore.ieee.org/document/133488>
- [16] G. Balestrino, et al. "Fast growth of Bi₂Sr₂Ca₂Cu₃O_{10+x} and Bi₂Sr₂CaCu₂O_{8+x} Thin-crystals at the surface of KCl fluxes," *Appl. Phys. Lett.*, vol. 64, no. 13, pp. 1735-1737, Mar 1994. doi: 10.1063/1.111794. [Online]. Available: <https://pubs.aip.org/aip/apl/article-abstract/64/13/1735/63016/Fast-growth-of-Bi2Sr2Ca2Cu3O10-x-and-Bi2Sr2CaCu2O8?redirectedFrom=fulltext>

- [17] X. L. Wang, J. Horvat, and H. K. Liu, and S. X. Dou, "Spiral growth of $\text{Bi}_2\text{Sr}_2\text{CaCu}_2\text{O}_y$ single crystals using KCl flux technique," *J. Cryst. Growth*, vol. 173, no. 3-4, pp. 380-385, Mar 1997. doi: 10.1016/S0022-0248(96)00906-2. [Online]. Available: <https://www.sciencedirect.com/science/article/abs/pii/S0022024896009062?via%3Dihub>
- [18] E. Juzeliunas and D. J. Fray, "Silicon electrochemistry in molten salts," *Chem. Rev.*, vol. 120, no. 3, pp. 1690-1709, Feb 2020. doi: 10.1021/acs.chemrev.9b00428. [Online]. Available: <https://pubs.acs.org/doi/10.1021/acs.chemrev.9b00428>
- [19] A. N. Salanov, et al., "Oxidation and recrystallization of platinum group metals (Pt, Pd, Rh) in oxygen. Surface and subsurface reconstruction of polycrystalline platinum during annealing in the O_2 atmosphere over the temperature range of 600–1400 K," *Appl. Surf. Sci.*, vol. 490, pp. 188-203, Oct 2019. doi: 10.1016/j.apsusc.2019.05.289. [Online]. Available: <https://www.sciencedirect.com/science/article/abs/pii/S0169433219315971?via%3Dihub>
- [20] M. T. Postek, "An approach to the reduction of hydrocarbon contamination in the scanning electron microscope," *Scanning*, vol. 18, no. 4, pp. 269-274, June 1996. doi: 10.1002/sca.1996.4950180402. [Online]. Available: <https://onlinelibrary.wiley.com/doi/10.1002/sca.1996.4950180402>
- [21] J. B. Nelson and D. P. Riley, "An experimental investigation of extrapolation methods in the derivation of accurate unit-cell dimensions of crystals," *Proc. Phys. Soc.*, vol. 57, no. 3, pp. 160-177, May 1945. doi: 10.1088/0959-5309/57/3/302. [Online]. Available: <https://iopscience.iop.org/article/10.1088/0959-5309/57/3/302>
- [22] P. Majewski, H. L. Su, and M. Quilitz, "Relationships between the chemical composition and properties of the high-temperature superconductor $\text{Bi}_{2+x}\text{Sr}_{2-y}\text{Ca}_{1+y}\text{Cu}_2\text{O}_{8+d}$," *J. Mater. Sci.*, vol. 32, no. 19, pp. 5137-5141, Oct 1997. doi: 10.1023/A:1018673602045. [Online]. Available: <https://link.springer.com/article/10.1023/A:1018673602045>
- [23] S. N. Zhang, C. S. Li, Q. B. Hao, J. Q. Feng, X. B. Ma, and P. X. Zhang, "Influences of Ca nonstoichiometry on the superconducting properties of Bi-2212 superconducting bulks," *J. Mater. Sci. Mater. Electron.*, vol. 26, no. 9, pp. 7214-7222, Sept 2015. doi: 10.1007/s10854-015-3347-y. [Online]. Available: <https://link.springer.com/article/10.1007/s10854-015-3347-y>
- [24] M. O. Rikel and E. E. Hellstrom, "Development of 2201 intergrowths during melt processing $\text{Bi}_{2212}/\text{Ag}$ conductors," *Physica C*, vol. 357-360, pp. 1081-1090, Aug 2001. doi: 10.1016/S0921-4534(01)00549-4. [Online]. Available: <https://www.sciencedirect.com/science/article/abs/pii/S0921453401005494?via%3Dihub>
- [25] F. Weitzer, W. Schnelle, R. C. Gil, S. Hoffmann, R. Gledigkeit, and Y. Grin, "Phase relationship and superconductivity in the Bi-rich part of the binary system Rh-Bi," *Calphad*, vol. 33, no. 1, pp. 27-30, Mar 2009. doi: 10.1016/j.calphad.2008.07.016. [Online]. Available: <https://www.sciencedirect.com/science/article/abs/pii/S0364591608000916?via%3Dihub>
- [26] D. F. Lupton, J. Merker, and F. Schölz, "The correct use of platinum in the XRF laboratory," *X-Ray Spectrom.*, vol. 26, no. 3, pp. 132-140, May 1997. doi: 10.1002/(SICI)1097-4539(199705)26:3<132::AID-XRS223>3.0.CO;2-L. [Online]. Available: [https://analyticalsciencejournals.onlinelibrary.wiley.com/doi/10.1002/\(SICI\)1097-](https://analyticalsciencejournals.onlinelibrary.wiley.com/doi/10.1002/(SICI)1097-)

4539(199705)26:3%3C132::AID-
XRS223%3E3.0.CO;2-L

- [27] Y. K. Taninouchi, R. Fujii, K. Sunagawa, T. H. Okabe, and H. Nakano, "High-temperature chlorination of rhodium using alkali-metal and alkaline-earth-metal chlorides," *Metall. Mater. Trans. B*, vol. 55, no. 6, pp. 4970-4980, Dec 2024. doi: 10.1007/s11663-024-03282-0. [Online]. Available: <https://link.springer.com/article/10.1007/s11663-024-03282-0>
- [28] O. V. Tokarev, D. S. Maltsev, and V. A. Volkovich, "Electrochemical properties of gallium in molten alkali metal chlorides," in *Proc. VII Int. Young Res. Conf. Phys. Technol. Innov. (PTI-2020)*, vol. 2313, 2020. doi: 10.1063/5.0032401. [Online]. Available: <https://pubs.aip.org/aip/acp/article-abstract/2313/1/020005/962150/Electrochemical-properties-of-gallium-in-molten?redirectedFrom=fulltext>
- [29] A. Yazdani, C. M. Howald, C. P. Lutz, A. Kapitulnik, and D. M. Eigler, "Impurity-induced bound excitations on the surface of $\text{Bi}_2\text{Sr}_2\text{CaCu}_2\text{O}_8$," *Phys. Rev. Lett.*, vol. 83, no. 1, pp. 176-179, July 1999. doi: 10.1103/PhysRevLett.83.176. [Online]. Available: <https://journals.aps.org/prl/abstract/10.1103/PhysRevLett.83.176>
- [30] S. Graser, P. J. Hirschfeld, T. Kopp, R. Gutser, B. M. Andersen, and J. Mannhart, "How grain boundaries limit supercurrents in high-temperature superconductors," *Nat. Phys.*, vol. 6, no. 8, pp. 609-614, Aug 2010. doi: 10.1038/nphys1687. [Online]. Available: <https://www.nature.com/articles/nphys1687>